Trajectory tracking and path following for under-actuated marine vehicles

C. Paliotta, *Student Member, IEEE,* E. Lefeber, *Member, IEEE,* K.Y. Pettersen, *Fellow, IEEE* J. Pinto, M. Costa and J. Sousa

***Abstract*—In this paper we present a control strategy for trajectory tracking and path following of generic paths for under-actuated marine vehicles. Our work is inspired and motivated by previous works on ground vehicles. In particular, we extend the definition of the *hand position* point, introduced for ground vehicles, to autonomous surface vehicles (ASVs) and autonomous underwater vehicles (AUVs) and then use the *hand position* point as output for a control strategy based on the input-output feedback linearization method. The presented strategy is able to deal with external disturbances affecting the vehicle, e.g. constant and irrotational ocean currents. Using Lyapunov analysis we are able to prove that the closed-loop system has an external dynamics which is globally exponentially stable (GES) and an internal dynamics which has ultimately bounded states, both for the trajectory tracking and the path following control problems. Finally, we present a simulation case study and experimental results in order to validate the theoretical results.**

I. Introduction

Autonomous vehicles have drawn the attention of researchers for the last decades. The use of autonomous vehicles is appealing for several real world applications. For instance, autonomous vehicles are particularly suitable for execution of tasks which are dull, hard or impossible to execute for humans. Furthermore, autonomous vehicles are interesting for different fields, and include unmanned vehicles for ground applications (unmanned ground vehicles-UGV), unmanned vehicles for aerial applications (unmanned aerial vehicles-UAV) and unmanned marine vehicles, that is, autonomous surface vehicles (ASV) and autonomous underwater vehicles (AUV). In each one of the aforementioned fields there are many examples of applications. We have autonomous cars which are leading towards profound changes in our concept of transportation [1, 2]. We have extensive use of UAVs for exploration, monitoring and surveillance tasks [3–5]. Also, autonomous vehicles have a large potential in applications intended to execute tasks in areas which are inaccessible for humans, for instance space exploration [6–8], and Arctic [9] or deep water exploration [10–12].

C. Paliotta, and K.Y. Pettersen are with Centre for Autonomous Marine Operations and Systems (NTNU AMOS), Department of Engineering Cybernetics, Norwegian University of Science and Technology, NO7491 Trondheim, Norway {claudio.paliotta, kristin.y.pettersen}@itk.ntnu.no

E. Lefeber is with Dynamics and Control Group at the Department of Mechanical Engineering, Eindhoven University of Technology P.O. Box 513, 5600 MB Eindhoven, the Netherlands A.A.J.Lefeber@tue.nl

J. Pinto, M. Costa and J.Sousa are with the Laboratrio de Sistemas e Tecnologia Subaqutica (LSTS), Faculdade de Engenharia da Universidade do Porto (FEUP), Porto, Portugal {zepinto,,mariacosta,jtasso}@fe.up.pt

This work was partly supported by the Research Council of Norway through the Centres of Excellence funding scheme, project No. 223254 NTNU AMOS.

Marine vehicles, both ASVs and AUVs, are generally characterized by challenging operational conditions. In fact, ocean currents and environmental disturbances, generally referred to as sea loads [13], may seriously influence the success of a mission. Furthermore, ASVs and AUVs are generally under-actuated vehicles, i.e., the number of independent control inputs is less than the degrees of freedom in the configuration space. This characteristic is due to common design rules. In fact, commercial marine vehicles are equipped just with fixed stern propellers and a steering rudder, or with two azimuth propellers. Sometimes they also have tunnel thrusters for lateral motion during docking, but such actuators work only at low speeds [14]. Consequently, the control design for this class of vehicles is challenging due to the absence of a direct actuation in the side direction (sway direction). The challenge is even harder when environmental disturbances affect the system.

Among the several control problems which are studied for marine vehicles, particularly interesting and challenging are the trajectory tracking and path following control problems. These are particularly relevant for several ASV and AUV applications, e.g., sea-bed scanning or pipeline inspection tasks [10]. The trajectory tracking control problem deals with the design of a controller which steers and stabilizes a vehicle to a geometric path that is parametrized in time, i.e., the vehicle has to follow a geometric path respecting a time constraint. Several works have dealt with this problem, proposing different approaches [15–25]. The work [21] presents a back-stepping controller for the trajectory tracking problem for an ASV. The result is extended in [22] considering the effect of environmental disturbances. The work [19] presents a Lyapunov's direct method approach to solve the trajectory tracking problem of ASVs. However, all [19, 21, 22] require the well-known condition of persistence of excitation (PE), i.e., the angular velocity of the vehicle has to be constantly excited. The controllers presented in [18, 20] do not need the PE condition.

The path following control problem differs from the trajectory tracking control problem because of the parametrization of the geometric path. That is, for the path following problem the path is left unparametrized [26–33] or parametrized by a parameter which is independent on the time [24, 34–37]. A well-known guidance control strategy for path following of straight lines is the line-of-sight (LOS) guidance [26, 27, 29, 38]. The LOS guidance is based on the approach of experienced helmsmen who steer the vessel towards a point lying at a constant distance ahead of the ship along the desired path. The LOS approach has been further improved with an integral action in order to be able to counteract environmental disturbances [28, 30, 39]. A LOS-like guidance approach for ASV to follow curved paths is presented in [37], where a linear observer is used to estimate and counteract the effect of an unknown constant ocean current. The work [37] is further developed in [24] where a different look-ahead distance for the LOS-like guidance is considered and a complete analysis of the zero dynamics of the system is presented.

The results presented in this paper are based on a different approach to the control problem of trajectory tracking and path following of marine vehicles. In fact, all the aforementioned works [18–24] have in common that the vehicle has to follow or track a path with respect to (w.r.t.) the center of mass or the pivot point. The latter is a point on the center-line of the vehicle such that its lateral motion (sway motion) is not affected by any of the control inputs. We here use a different approach where we extend the definition of *hand position*, which has been used for ground vehicles in [40, 41], to marine vehicles. The definition of the *hand position* is further discussed below, but briefly described it is a point lying along the center-line of the vehicle ahead of the pivot point. Choosing the hand position motion as output of our system and using an input-output feedback linearizing controller, we perform a change of inputs to our system, which, as typical for feedback-linearized systems, leads to an external dynamics which is linear, and in particular to a double integrator. Having a linear external dynamics facilitates the control design, and one of our motivations for this is that it is then possible to apply well developed formation control strategies for multi-agent systems consisting of under-actuated marine vehicles, a topic within which there exists very few results. One example of the usefulness of this approach is given in [42], where we have presented a synchronization strategy for marine vehicles based on the *hand position* point and the input-output feedback linearizing controller presented in [43]. The price to pay for a linear external dynamics is a nonlinear internal dynamics which is affected by the states of the external dynamics.

In this paper we consider the model of an ASV or an AUV moving in the horizontal plane affected by an environmental disturbance, i.e., an unknown constant ocean current. Note that, as opposed to UGVs which can be described by a kinematic model, for ASVs and AUVs we need to consider also the dynamics, since these vehicles have uncontrolled dynamics. Furthermore, for marine vehicles the effect of ocean currents are significant, and the control approach therefore needs to handle environmental disturbances. We address the problem of trajectory tracking and path following control for straight lines and curved paths. For the path following case we present a novel parametrization of the path that is dependent on the distance of the vehicle from the path. The proposed control strategy is based on the definition of the *hand position* point and an input-output feedback linearizing controller. We present a change of coordinates which is not standard for the input-output feedback linearizing approach, but that allows us to obtain a transformed model where the ocean current affects the system at the level of the linear external dynamics and can be counteracted with a simple integral action. We show that the integral state is able to give an estimate of the ocean current. We prove that our output, i.e., the *hand position* point, converges to the desired trajectory (or path) globally exponentially while the states of the internal dynamics are ultimately bounded. We show also that for the case of straight line paths we have *almost*-global asymptotic stability (AGAS) of the closed-loop system. Preliminary results have been presented in [43], while we here extend these from straight line to generic paths and include a new strategy for the path following control problem. Then, we present simulation and experimental results performed using the lightweight autonomous underwater vehicle (LAUV) of the University of Porto [44]. In particular, we present a simulation case study concerning the trajectory tracking control problem where we consider a lawn-mower path made of straight lines and circular arcs. Finally, we present experimental results from a sea trial performed using the LAUV. In particular, we first present the result of a simulation performed using the simulator of DUNE, software running on the LAUV [45]. The simulation was performed prior the sea trials in order to verify that the vehicle was correctly behaving after that the proposed control law was implemented. The simulation case study in DUNE is also used as a benchmark for the results of a sea trial performed in the harbor Porto, Portugal.

The paper is organized as follows: Section II presents the model of the class of vehicles which we consider; in Section III we describe our control approach; in Section IV we formalize the trajectory tracking control problem and give the control objectives; Section V presents the proposed controller; in Section VI we present the main result for trajectory tracking in the form of a theorem and present a rigorous mathematical proof; then Section VII presents our approach applied to the path following problem, our proposed strategy and the result in the form of a theorem together with a rigorous proof; in Section VIII we present simulation results concerning the trajectory tracking control problem. Section IX presents the experimental results; finally in Section X the conclusions are given.

II. Vehicle Model

This section briefly describes the 3 degrees of freedom (DOF) maneuvering model for the motion of an ASV or an AUV moving in the horizontal plane. For more details the reader is referred to [38].

First, we list the assumptions valid for the model.

A. Assumptions

Assumption 1. *The motion of the vehicle is described in 3 DOF, i.e., surge, sway, yaw.*

Assumption 2. *The vehicle is port-starboard symmetric.*

Assumption 3. *The hydrodynamic damping is linear.*

Remark 1. *Nonlinear damping is not considered since it would increase the complexity of the controller without contributing to improving the result. In particular, the nonlinear*

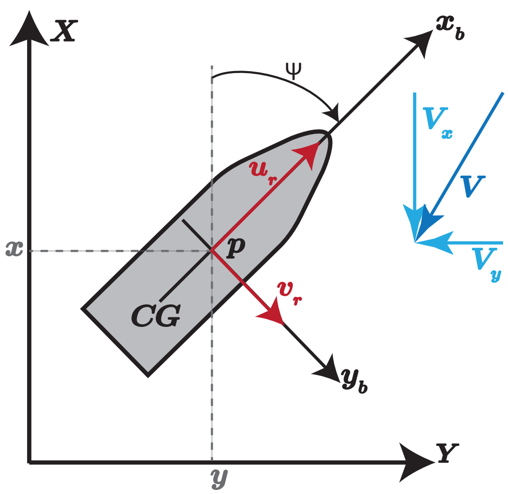

Fig. 1: Vehicles' states.

damping forces have a passive nature, and therefore the stability of the vehicle will be further improved by the nonlinear damping.

Assumption 4. *The ocean current in the inertial frame* $\mathbf{V} = [V_x, V_y]^T$ *is constant, irrotational and bounded, i.e.,* $\exists V_{\max} > 0$ *such that* $\sqrt{V_x^2 + V_y^2} \leq V_{\max}$.

B. The Vessel Model

The *North-East-Down* (NED) frame convention [38] for the inertial frame I is used. The position and the orientation of the vehicle, i.e., the pose, in the NED frame are given by the vector $\eta = [x, y, \psi]^T$. The velocities in the body frame are given by $\nu = [u, v, r]^T$, which are the surge velocity, the sway velocity and the yaw rate, respectively (see Figure 1). The rotation between the body frame and the inertial frame is given by the rotation matrix $\mathbf{R}$

$$\mathbf{R} = \begin{bmatrix} \cos(\psi) & -\sin(\psi) & 0 \\ \sin(\psi) & \cos(\psi) & 0 \\ 0 & 0 & 1 \end{bmatrix}. \tag{1}$$

The vector $\mathbf{V} = [V_x, V_y, 0]^T$ represents the ocean current in the NED frame. In the body frame we have that the ocean current is $\mathbf{v}_c = \mathbf{R}^T\mathbf{V}$. The motion of an ASV or an AUV moving in a horizontal plane, is given by the following 3 DOF maneuvering model given in [38]:

$$\dot{\eta} = \mathbf{R}\nu_r + \mathbf{V} \tag{2a}$$

$$\mathbf{M}\dot{\nu}_r + \mathbf{C}(\nu_r)\nu_r + \mathbf{D}\nu_r = \mathbf{Bf}, \tag{2b}$$

where $\nu_r = [u_r, v_r, r]^T = \nu - \mathbf{v}_c$ is the vector of the relative velocities in the body frame. Then $\mathbf{f} = [T_u, T_r]^T$, where T_u is the thruster force and T_r is the rudder angle. Note that $\mathbf{f} \in \mathbb{R}^2$ and therefore the vehicle is under-actuated in its configuration space $\mathbb{R}^3$. According to Assumptions 1-3, the matrices $\mathbf{M}, \mathbf{D}, \mathbf{B}$ have the following structure

$$\mathbf{M} \triangleq \begin{bmatrix} m_{11} & 0 & 0 \\ 0 & m_{22} & m_{23} \\ 0 & m_{23} & m_{33} \end{bmatrix}; \ \mathbf{D} \triangleq \begin{bmatrix} d_{11} & 0 & 0 \\ 0 & d_{22} & d_{23} \\ 0 & d_{32} & d_{33} \end{bmatrix}; \ \mathbf{B} \triangleq \begin{bmatrix} b_{11} & 0 \\ 0 & b_{22} \\ 0 & b_{32} \end{bmatrix}. \tag{3}$$

The mass matrix $\mathbf{M} = \mathbf{M}^T > 0$ includes the hydrodynamic added mass. The matrix $\mathbf{D}$ gives the linear damping coefficients, and $\mathbf{B} \in \mathbb{R}^{3\times 2}$ is the actuator configuration matrix. The Coriolis matrix $\mathbf{C}$, which includes the Coriolis and centripetal effects, can be derived from $\mathbf{M}$ as shown in [38]. For the body fixed frame b we consider the following assumption to hold

Assumption 5. *The body-fixed coordinate frame b (body frame) is located at a point $(x_P^*, 0)$, at a distance x_P^* from the vehicle's center of gravity (CG) along the center-line of the ship. This point $(x_P^*, 0)$ is chosen to be the pivot point, i.e., such that $\mathbf{M}^{-1}\mathbf{B}f = [\tau_u, 0, \tau_r]^T$ when the model (2) is written w.r.t. this point.*

Remark 2. *The pivot point $(x_P^*, 0)$ satisfying Assumption 5 always exists for ships and AUVs with the center of mass located on the centerline of the vehicle [38]. This is implied by Assumption 2. Furthermore, the body-fixed frame can be translated to a desired location x_P^* [38].*

For convenience, we rewrite (2) in component form

$$\dot{x} = u_r\cos(\psi) - v_r\sin(\psi) + V_x \tag{4a}$$
$$\dot{y} = u_r\sin(\psi) + v_r\cos(\psi) + V_y \tag{4b}$$
$$\dot{\psi} = r \tag{4c}$$
$$\dot{u}_r = F_{u_r}(v_r) + \tau_u \tag{4d}$$
$$\dot{v}_r = X(u_r)r + Y(u_r)v_r \tag{4e}$$
$$\dot{r} = F_r(u_r, v_r, r) + \tau_r. \tag{4f}$$

The expressions for $F_{u_r}(u_r), F_r(u_r, v_r, r)$ are given in Appendix A. Furthermore, $X(u_r) = -X_1 u_r + X_2$, $Y(u_r) = -Y_1 u_r - Y_2$ and X_1, X_2, Y_1, Y_2 are reported in Appendix A. We consider the following assumption to hold:

Assumption 6. *The following bounds hold on Y_1, Y_2*

$$Y_1 > 0, \qquad Y_2 > 0. \tag{5}$$

Remark 3. *Note that $Y_1, Y_2 > 0$ implies $Y(u_r) < 0$. This is a natural assumption since $Y(u_r) \geq 0$ corresponds to the situation of unstable sway dynamics. That is, a small perturbation applied along the sway direction would cause an undamped motion, which is unfeasible for commercial marine vehicles by design.*

III. Hand Position: Line of Reasoning

Before describing the trajectory tracking problem, in this section we present our different approach to the general control problem of a marine vehicle. In particular, we present the considerations which justify a different choice of the output for the system described by (4) compared to previous literature. In previous works on trajectory tracking of ASVs and AUVs the output of the system has been chosen as either the center of mass or the pivot point $\mathbf{p} = [x, y]^T$, which was then defined as the origin of the body-fixed frame (cf. Fig. 2). Inspired by the work of Lawton and Beard [41], we choose the motion of a certain point on the center line of the vehicle, which we call the *hand position*, as the output of the system.

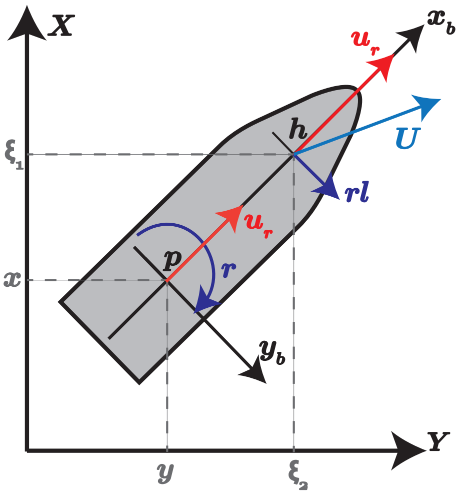

Fig. 2: The hand position point.

The work [41] deals with the control problem of first-order non-holonomic vehicles, in particular unicycles whose model is

$$\dot{x} = u_1 \cos(\psi) \tag{6a}$$
$$\dot{y} = u_1 \sin(\psi) \tag{6b}$$
$$\dot{\psi} = u_2. \tag{6c}$$

where u_1, u_2 are the control inputs, $\mathbf{p}_{gv} = [x, y]^T$ is the position in the global frame and ψ is the yaw angle. In particular, u_1 is the forward velocity and u_2 is the yaw rate. The model (6) is similar to (4a-4c). They differ just because of the under-actuated state v_r which is characterized by the uncontrolled dynamics (4e), and because of the ocean current that affects the system. Note also that (4) has control inputs in the surge and yaw directions like in (6), but on the dynamic level instead of on a purely kinematic level.

The aforementioned similarities between the kinematic model of unicycles and ASVs and AUVs motivate us to choose a different output from the commonly used pivot point for AUVs and ASVs. Based on this, we extend the definition of the *hand position* point to marine vehicles and similarly to [41] by defining $\mathbf{h} = [\xi_1, \xi_2]^T$ with

$$\xi_1 = x + l\cos(\psi) \qquad \xi_2 = y + l\sin(\psi), \tag{7}$$

where x, y give the position of the pivot point in the NED frame, ψ is the yaw angle and $l > 0$ is a constant. An illustration of the hand position point is given in Figure 2. For practical applications the constant l may be chosen such that the point $\mathbf{h}$ coincides with the position of a certain sensor of the vehicle. For instance, in case of an exploration mission, $\mathbf{h}$ may be chosen similar to the position of a camera, such that $\mathbf{h}$ tracks a prescribed path in order to take specific images of the area which is explored. From Figure 2 it is also clear that the point $\mathbf{h}$ is indirectly actuated by the control inputs acting on $\mathbf{p}$. In particular, note that an actuation on $\mathbf{p}$ along the surge direction generates an actuation in the surge direction of $\mathbf{h}$. Then, an actuation around the yaw axis in $\mathbf{p}$ generates an actuation in the sway direction of $\mathbf{h}$, which is directly proportional to the constant l. Note that we therefore have two indirect control inputs available which actuate the point $\mathbf{h}$ with a linear motion in two perpendicular directions, while in $\mathbf{p}$ we have available two control inputs which generate motion in the linear direction of surge and in the rotational direction of yaw, respectively.

The next step is to apply the output feedback linearization method [46] with $\mathbf{h}$ chosen as output. Note, however, that the input-output feedback linearization method [46] cannot be straightforwardly applied, but needs to be adjusted because of the unknown ocean current that affects the system. This adjustment is described later in this section. First, we need to check if (4) is input-output feedback linearizable with output $\mathbf{h}$, i.e, we need to check if the vector relative degree $\rho = [\rho_{\xi_1}, \rho_{\xi_2}]^T$ is well defined [46] . Deriving ξ_1, ξ_2 twice we obtain

$$\begin{bmatrix} \ddot{\xi}_1 \\ \ddot{\xi}_2 \end{bmatrix} = \begin{bmatrix} \cos(\psi) & -\sin(\psi) \\ \sin(\psi) & \cos(\psi) \end{bmatrix} \begin{bmatrix} F_u(v,r) - vr - lr^2 \\ ur + X(u)r + Y(u)v + F_r(u,v,r)l \end{bmatrix} + \underbrace{\begin{bmatrix} \cos(\psi) & -l\sin(\psi) \\ \sin(\psi) & l\cos(\psi) \end{bmatrix}}_{\mathbf{B}(\psi)} \begin{bmatrix} \tau_u \\ \tau_r \end{bmatrix}. \tag{8}$$

From (8), we see that the system has a well-defined vector relative degree since $\rho_{\xi_1} = \rho_{\xi_2} = 2$ for $l \neq 0$, since $\mathbf{B}(\psi)$ is non-singular for $l \neq 0$. Note that $l = 0$ makes $\mathbf{B}(\psi)$ singular and therefore the system does not have a well-defined relative degree when the pivot point is chosen as output.

Now we define the following change of coordinates

$$z_1 = \psi \tag{9a}$$
$$z_2 = r \tag{9b}$$
$$\xi_1 = x + l\cos(\psi) \tag{9c}$$
$$\xi_2 = y + l\sin(\psi) \tag{9d}$$
$$\xi_3 = u_r\cos(\psi) - v_r\sin(\psi) - rl\sin(\psi) \tag{9e}$$
$$\xi_4 = u_r\sin(\psi) + v_r\cos(\psi) + rl\cos(\psi). \tag{9f}$$

Note that we cannot choose $\xi_3 = \dot{\xi}_1, \xi_4 = \dot{\xi}_2$ since this choice would imply that ξ_3, ξ_4 are functions of the ocean current, which is unknown. Our change of coordinates results in $\xi_3 = \dot{\xi}_1 - V_x, \xi_4 = \dot{\xi}_2 - V_y$. Thus, ξ_3, ξ_4 are the relative velocities of the vehicle in the global frame.

Applying (9), (4) becomes

$$\dot{z}_1 = z_2 \tag{10a}$$
$$\dot{z}_2 = F_{z_2}(z_1, \xi_3, \xi_4) + \tau_r \tag{10b}$$
$$\begin{bmatrix} \dot{\xi}_1 \\ \dot{\xi}_2 \end{bmatrix} = \begin{bmatrix} \xi_3 \\ \xi_4 \end{bmatrix} + \begin{bmatrix} V_x \\ V_y \end{bmatrix} \tag{10c}$$
$$\begin{bmatrix} \dot{\xi}_3 \\ \dot{\xi}_4 \end{bmatrix} = \begin{bmatrix} F_{\xi_3}(z_1, \xi_3, \xi_4) \\ F_{\xi_4}(z_1, \xi_3, \xi_4) \end{bmatrix} + \begin{bmatrix} \cos(z_1) & -l\sin(z_1) \\ \sin(z_1) & l\cos(z_1) \end{bmatrix} \begin{bmatrix} \tau_u \\ \tau_r \end{bmatrix} \tag{10d}$$

where

$$\begin{bmatrix} F_{\xi_3}(\cdot) \\ F_{\xi_4}(\cdot) \end{bmatrix} = \begin{bmatrix} \cos(\psi) & -\sin(\psi) \\ \sin(\psi) & \cos(\psi) \end{bmatrix} \begin{bmatrix} F_{u_r}(\cdot) - v_r r - lr^2 \\ u_r r + X(\cdot)r + Y(\cdot)v_r + F_r(\cdot)l \end{bmatrix} \tag{11}$$

and $F_{z_2}(z_1, \xi_3, \xi_4)$ is obtained from $F_r(u_r, v_r, r)$ substituting $u_r = \xi_3\cos(z_1) + \xi_4\sin(z_1)$, $v_r = -\xi_3\sin(z_1) + \xi_4\cos(z_1) - z_2 l$, and $r = z_2$. Note that choosing $\xi_3 \neq \dot{\xi}_1, \xi_4 \neq \dot{\xi}_2$ in (9) is not a standard approach for input-output linearization. However, this choice is necessary to make ξ_3, ξ_4 independent on the unknown ocean current. Note also that with this choice for ξ_3, ξ_4 the environmental disturbance is affecting the system at the level of the linear external dynamics where, as it becomes clear from the next sections, it is possible to counteract it using an integral action.

Now we apply the following change of input in order to linearize the external dynamics

$$\begin{bmatrix}\tau_u\\ \tau_r\end{bmatrix} = \begin{bmatrix}\cos(\psi) & -l\sin(\psi)\\ \sin(\psi) & l\cos(\psi)\end{bmatrix}^{-1}\begin{bmatrix}-F_{\xi_3}(z_1,\xi_3,\xi_4)+\mu_1\\ -F_{\xi_4}(z_1,\xi_3,\xi_4)+\mu_2\end{bmatrix}. \quad (12)$$

The terms μ_1, μ_2 in (12) are new inputs which are to be defined in Section V in order to solve the trajectory tracking problem. Substituting (12) in (10) we obtain

$$\begin{aligned}
\dot z_1 =& z_2 && (13a)\\
\dot z_2 =& -\left(\left(Y_1 - \tfrac{X_1-1}{l}\right)U\cos(z_1-\phi) + Y_2 + \tfrac{X_2}{l}\right)z_2\\
&-\left(\tfrac{Y_1}{l}U\cos(z_1-\phi)+\tfrac{Y_2}{l}\right)U\sin(z_1-\phi)\\
&-\tfrac{\mu_1\sin(z_1)}{l}+\tfrac{\mu_2\cos(z_1)}{l} && (13b)\\
\dot\xi_1 =& \xi_3 + V_x && (13c)\\
\dot\xi_2 =& \xi_4 + V_y && (13d)\\
\dot\xi_3 =& \mu_1 && (13e)\\
\dot\xi_4 =& \mu_2 && (13f)
\end{aligned}$$

where

$$U = \sqrt{\xi_3^2+\xi_4^2}, \quad \phi = \operatorname{atan2}\left(\frac{\xi_4}{\xi_3}\right). \quad (14)$$

Note that z_1 appears only as an argument of trigonometric functions with period 2π. Therefore, we can consider (13a-13b) to take values on the manifold $\mathbb{M} = \mathbb{S}\times\mathbb{R}$ where $\mathbb{S}$ is the one-dimensional sphere.

The main advantage of choosing $\mathbf{h}$ as output is clear from (13). The transformed model (13) is characterized by a linear external dynamics (13c-13f) and a nonlinear internal dynamics (13a-13b) as common for input-output linearized systems. Thus, as opposed to considering the model (2), we can consider the external dynamics, which is linear, for control purposes. The drawback is clearly the fact that the inputs μ_1, μ_2, which are to be designed in order to fulfill the control objectives, are affecting also the internal dynamics (13a-13b), and we have to carefully check the internal stability properties of the states z_1, z_2.

IV. Control Objectives

In this section the trajectory tracking control problem is formalized. Based on the arguments in Section III, our control objective is to make the point $\mathbf{h}$ follow an assigned generic trajectory. Without loss of generality we consider a trajectory which starts at the origin of the NED frame. We consider the desired trajectory $\Gamma(t) = \{(\xi_{1_d}(t), \xi_{2_d}(t), \xi_{3_d}(t), \xi_{4_d}(t)) | t \in \mathbb{R}^+\}$ to be parametrized by the time t and where $\dot\xi_{1_d} = \xi_{3_d}$, $\dot\xi_{2_d} = \xi_{4_d}$. We consider the following to hold:

Assumption 7. *There exist constants* $\underline{\xi}_3, \bar\xi_3, \underline{\xi}_4, \bar\xi_4, \underline{\xi}^*_{3_d}, \bar\xi^*_{3_d}, \underline{\xi}^*_{4_d}, \bar\xi^*_{4_d}$ *such that*

$$\begin{aligned}
\underline{\xi}_3 \le& \xi_{3_d}(t) \le \bar\xi_3 && (15a)\\
\underline{\xi}_4 \le& \xi_{4_d}(t) \le \bar\xi_4 && (15b)\\
\underline{\xi}^*_{3_d} \le& \dot\xi_{3_d}(t) \le \bar\xi^*_{3_d} && (15c)\\
\underline{\xi}^*_{4_d} \le& \dot\xi_{4_d}(t) \le \bar\xi^*_{4_d}. && (15d)
\end{aligned}$$

Remark 4. *Assumption 7 implies that the desired linear velocity and acceleration of the vehicle are upper and lower bounded. The lower bound on the velocity is necessary for the under-actuated vehicle to be controllable. The upper bound on the velocity is required for the desired linear velocity to be bounded, and thus create a feasible trajectory. The bounds on the acceleration imply a smooth motion of the vehicle.*

The control objectives can be formalized as

$$\begin{aligned}
&\lim_{t\to\infty}(\xi_1 - \xi_{1_d}(t)) = 0 && (16a)\\
&\lim_{t\to\infty}(\xi_2 - \xi_{2_d}(t)) = 0 && (16b)\\
&\lim_{t\to\infty}(\xi_3 - (\xi_{3_d}(t) - V_x)) = 0 && (16c)\\
&\lim_{t\to\infty}(\xi_4 - (\xi_{4_d}(t) - V_y)) = 0. && (16d)
\end{aligned}$$

Note that (16c-16d) require the relative velocities ξ_3, ξ_4 in the global frame to converge to the values $\xi_{3_d} - V_x, \xi_{4_d} - V_y$. This is necessary because we want the absolute velocities in the NED frame to converge to ξ_{3_d}, ξ_{4_d}, which allow the vehicle to track the desired trajectory $\Gamma(t)$. Note that (16c-16d) depend on V_x, V_y which are unknown. As discussed in Section I, we handle this by introducing an integral action in our controller.

We consider the following assumption to hold

Assumption 8. *The desired total relative velocity is chosen such that* $U_d = \sqrt{(\xi^2_{3_d} - V_x)^2 + (\xi_{4_d} - V_y)^2} > 0$. *Furthermore, the vehicle's thrusters provide enough power to overcome the ocean current disturbance.*

Remark 5. *This is assumption is needed in order to have forward motion of the vehicle, which again is needed for the controllability of under-actuated marine vehicles.*

Remark 6. *Note that Assumptions 4 and 7 imply that* $\underline{U}_d \le U_d \le \bar U_d$ *and* $\underline{U}^*_d \le \dot U_d \le \bar U^*_d$, *where* $\underline{U}_d$, $\bar U_d$, $\underline{U}^*_d$, $\bar U^*_d$ *are constants.*

V. The Controller

In this section we present our choice for the control inputs $\mu = [\mu_1, \mu_2]^T$ in (13) which solve the control problem described in Section IV. In order to make the point $\mathbf{h}$ track the desired trajectory $\Gamma(t)$ we choose

$$\begin{aligned}
\mu_1 =& -k_{v_x}(\xi_3 - \xi_{3_d}) - k_{p_x}(\xi_1 - \xi_{1_d})\\
&- k_{I_x}(\xi_{1_I} - \xi_{1_{d_I}}) + \dot\xi_{3_d} && (17a)\\
\mu_2 =& -k_{v_y}(\xi_4 - \xi_{4_d}) - k_{p_y}(\xi_2 - \xi_{2_d})\\
&- k_{I_y}(\xi_{2_I} - \xi_{2_{d_I}}) + \dot\xi_{4_d} && (17b)
\end{aligned}$$

where $k_{p_x}, k_{p_y}, k_{v_x}, k_{v_y}, k_{I_x}, k_{I_y}$ are positive real gains, $\xi_{i_I} = \int_0^t \xi_i(\tau)\mathrm{d}\tau$ where $i \in \{1, 2, 1_d, 2_d\}$. The integral action in (17) is needed to reject the constant disturbance, i.e., the ocean current $\mathbf{V}$, affecting the system [47].

VI. Main Result

This section presents the main result. The following theorem gives the conditions under which the control objectives (16a) are fulfilled using the controller (12).

Theorem 1. *Consider an under-actuated marine vehicle described by the model* (4)*. Consider the hand position point* $\mathbf{h} = [\xi_1, \xi_2]^T = [x + l\cos(\psi), y + l\sin(\psi)]^T$*, where* $[x, y]^T$ *is the position of the pivot point of the ship,* l *is a positive constant and* ψ *is the yaw angle of the vehicle. Then define* $U_d = \sqrt{(\xi_{3_d} - V_x)^2 + (\xi_{4_d} - V_y)^2} > 0$ *as the desired relative velocity magnitude and* $\phi_1 = \arctan\left(\frac{\xi_{4_d} - V_y}{\xi_{3_d} - V_x}\right)$ *as the crab angle. If Assumptions 1-8 are satisfied and if*

$$
\begin{aligned}
0 <&\bar{U}_d < \tfrac{Y_2}{Y_1} && (18)\\
k_{v_i} >&0,\ k_{p_i} > 0,\ k_{I_i} > 0,\ i \in \{x, y\} && (19)\\
k_{v_i}k_{p_i} >&k_{I_i} \quad i \in \{x, y\} && (20)\\
l >& \max\left\{\frac{m_{22}}{m_{23}}, -\frac{X_2}{Y_2}\right\} && (21)\\
\bar{U}_d^* \leq& \frac{2\min\{\underline{a}(\underline{d} - \underline{c}), b\}}{\frac{Y_1\bar{U}_d}{l} + 2\left(Y_1 - \frac{X_1 - 1}{l}\right)} && (22)
\end{aligned}
$$

then the controller (12)*, where the new inputs* μ_1, μ_2 *are given by* (17)*, guarantees the achievement of the control objectives* (16)*. In particular,* $(\xi_1, \xi_2, \xi_3, \xi_4) \rightarrow (\xi_{1_d}, \xi_{2_d}, \xi_{3_d}, \xi_{4_d})$ *globally exponentially and* (z_1, z_2) *are globally ultimately bounded. Furthermore, the steady state values of the integral variables give an estimate of the ocean current:*

$$
\hat{V}_x = \lim_{t\to\infty} \frac{k_{v_x}(\xi_{1_I}(t) - \xi_{1_{I_d}}(t))}{k_{I_x}} \tag{23a}
$$

$$
\hat{V}_y = \lim_{t\to\infty} \frac{k_{v_y}(\xi_{2_I}(t) - \xi_{2_{I_d}}(t))}{k_{I_y}}. \tag{23b}
$$

Remark 7. *Notice that we assume an unknown ocean current and therefore also the crab angle* ϕ*, which is necessary in order to counteract the currents and follow the trajectory, is unknown. However, the integral action in* (12) *takes care of compensating for the unknown value of the constant disturbance.*

Proof. We define the following change of coordinates

$$
\tilde{z}_1 = z_1 - \phi_1,\ \tilde{\xi}_{1_I} = \xi_{1_I} - \int_0^t \xi_{1_d}\mathrm{d}\tau - \frac{k_{I_x}V_x}{k_{v_x}}, \tag{24a}
$$

$$
\tilde{z}_2 = z_2 - \dot{\phi}_1,\ \tilde{\xi}_{2_I} = \xi_{2_I} - \int_0^t \xi_{2_d}\mathrm{d}\tau - \frac{k_{I_y}V_y}{k_{v_y}}, \tag{24b}
$$

$$
\tilde{\xi}_1 = \xi_1 - \xi_{1_d},\ \tilde{\xi}_4 = \xi_4 - (\xi_{4_d} - V_y), \tag{24c}
$$

$$
\tilde{\xi}_2 = \xi_2 - \xi_{2_d},\ \tilde{\xi}_3 = \xi_3 - (\xi_{3_d} - V_x). \tag{24d}
$$

Defining the vectors $\tilde{z} = [\tilde{z}_1, \tilde{z}_2]^T$, $\tilde{z}_s = [\sin(\tilde{z}_1), \tilde{z}_2]^T$, $\tilde{\xi} = [\tilde{\xi}_{1_I}, \tilde{\xi}_{2_I}, \tilde{\xi}_1, \tilde{\xi}_2, \tilde{\xi}_3, \tilde{\xi}_4]^T$, the closed-loop system becomes

$$
\dot{\tilde{z}} = H_{\tilde{z}}(\tilde{z}_1)\tilde{z}_s + G(\tilde{z}, \tilde{\xi}_3, \tilde{\xi}_4)\tilde{\xi} + \Delta(\dot{\phi}_1, \ddot{\phi}_1, \tilde{z}_1) \tag{25a}
$$

$$
\dot{\tilde{\xi}} = H_{\tilde{\xi}}\tilde{\xi} \tag{25b}
$$

where $G(\cdot)$ is reported in Appendix A and

$$
H_{\tilde{z}}(\tilde{z}) = \begin{bmatrix} 0 & 1 \\ -(c\cos(z_1) + d) & -(a\cos(z_1) + b) \end{bmatrix} \tag{26}
$$

$$
\Delta(\dot{\phi}_1, \ddot{\phi}_1, \tilde{z}_1) = \begin{bmatrix} 0 \\ \delta(\dot{\phi}_1, \ddot{\phi}_1, \sin(\tilde{z}_1)) \end{bmatrix} \tag{27}
$$

$$
\begin{aligned}
\delta(\cdot) =& -(a\cos(\tilde{z}_1) + b)\dot{\phi}_1 + \ddot{\phi}_1 \\
&+ (\dot{\xi}_{4_d}\cos(\tilde{z}_1) - \dot{\xi}_{3_d}\sin(\tilde{z}_1))\cos(\phi_1) \\
&+ (-\dot{\xi}_{4_d}\sin(\tilde{z}_1) + \dot{\xi}_{3_d}\cos(\tilde{z}_1))\sin(\phi_1)
\end{aligned} \tag{28}
$$

$$
a = \left(Y_1 - \frac{X_1 - 1}{l}\right)U_d \qquad b = Y_2 + \frac{X_2}{l} \tag{29}
$$

$$
c = \frac{Y_1 U_d^2}{l} \qquad d = \frac{Y_2 U_d}{l} \tag{30}
$$

$$
H_{\tilde{\xi}} = \begin{bmatrix} 0 & 0 & 1 & 0 & 0 & 0 \\ 0 & 0 & 0 & 1 & 0 & 0 \\ 0 & 0 & 0 & 0 & 1 & 0 \\ 0 & 0 & 0 & 0 & 0 & 1 \\ -k_{I_x} & 0 & -k_{p_x} & 0 & -k_{v_x} & 0 \\ 0 & -k_{I_y} & 0 & -k_{p_y} & 0 & -k_{v_y} \end{bmatrix}. \tag{31}
$$

Assumption 6 implies $c, d > 0$ and (18) implies $d > c\ \forall t$. We also have $a, b > 0\ \forall t$ because of (21). Note also that from $\underline{U}_d \leq U_d \leq \bar{U}_d$ we have $\bar{a} > a > \underline{a}, \bar{c} > c > \underline{c}, \bar{d} > d > \underline{d}$ with $\bar{a}, \underline{a}, \bar{c}, \underline{c}, \bar{d}, \underline{d}$ positive constants. Finally, we have also that $\delta \leq \bar{\delta}$ since δ is a continuous function of bounded signals. We now study the stability properties of the external dynamics (25b) and the tracking dynamics (Equation (25a) with $G(\tilde{z}, \tilde{\xi}_3, \tilde{\xi}_4)\tilde{\xi} = 0$) and then the stability properties of the total system (25).

The external dynamics

The equilibrium point of (25b) is $\tilde{\xi} = \mathbf{0}$. The matrix $H_{\tilde{\xi}}$ is Hurwitz for $k_{v_i}, k_{p_i}, k_{I_i}$ respecting (19-20).

Remark 8. *From the integral states we obtain an estimate of the unknown ocean current when the steady state condition is reached. In particular, we have* (23)*.*

The tracking dynamics

Consider the

$$
\dot{\tilde{z}}_1 = \tilde{z}_2 \tag{32a}
$$

$$
\begin{aligned}
\dot{\tilde{z}}_2 =& -(a\cos(\tilde{z}_1) + b)\tilde{z}_2 - (c\cos(\tilde{z}_1) + d)\sin(\tilde{z}_1) \\
&+ \delta(\dot{\phi}_1, \ddot{\phi}_1, \tilde{z}_1).
\end{aligned} \tag{32b}
$$

The subsystem (32) does not have an equilibrium point at the origin due to the disturbance $\delta(\cdot)$. Thus, we study the ultimately boundedness of the states $\tilde{z}_1, \tilde{z}_2$.

Define the following Lyapunov function candidate (LFC) for (32)

$$
W = \frac{1}{2}\tilde{z}_s^T \underbrace{\begin{bmatrix} a^2+c & a \\ a & 1 \end{bmatrix}}_{P_{z_s}} \tilde{z}_s + (ab + d)(1 - \cos(\tilde{z}_1)). \tag{33}
$$

We have that $W > 0\ \forall(\cos(\tilde z_1), \sin(\tilde z_1), \tilde z_2) \in \mathbb{M} - \{[1,0,0]\}$ and $W = 0$ only for $(\cos(\tilde z_1), \sin(\tilde z_1), \tilde z_2) = (1,0,0)$. The time derivative is

$$\begin{aligned}\dot W =& -\tilde z_s^T \begin{bmatrix} a(d + c\cos(\tilde z_1)) & 0 \\ 0 & b\end{bmatrix}\tilde z_s + \frac{\partial W}{\partial \tilde z_s}\Delta_{\tilde z} \\ &+ \tilde z_s^T \begin{bmatrix} 2\dot a a + \dot c & \dot a \\ \dot a & 0\end{bmatrix}\tilde z_s + (\dot a b + \dot d)(1-\cos(\tilde z_1)).\end{aligned} \tag{34}$$

Note that $\dot a$, $\dot c$, $\dot d$ all depend on $\dot U_d$. Since $\dot U_d \leq \bar U_d^*$ due to Assumptions 7-8, we have $|\dot a| \leq \bar a^*$, $|\dot c| \leq \bar c^*$, $|\dot d| \leq \bar d^*$. Then we have

$$\begin{aligned}\dot W \leq& -\tilde z_s^T \underbrace{\left[\begin{smallmatrix} a(d-c) & 0 \\ 0 & b\end{smallmatrix}\right]}_{Q_{\tilde z}}\tilde z_s + \frac{\partial W}{\partial \tilde z_s}\Delta_{\tilde z} \\ &\underbrace{\frac{1}{2}\left(|2\dot a + \dot c| + |\dot a|\right)}_{\omega}\|\tilde z_s\|^2 + (\bar a^* b + \bar d^*)(1-\cos(\tilde z_1)).\end{aligned} \tag{35}$$

From the definition of $\Delta_{\tilde z}$ we have that

$$\left\|\frac{\partial W}{\partial \tilde z_s}\right\| \|\Delta_{\tilde z}\| \leq \alpha_1 \bar\delta \|\tilde z_s\| \tag{36}$$

where $\alpha_1 = \max\{1, a\}$ and $\bar\delta$ is the upperbound of $\delta(t)$, i.e. $\delta(t) \leq \bar\delta$ since $\delta(t)$ is function of bounded signals. Then we obtain

$$\dot W \leq -\underbrace{\left(\lambda_{Q_{\tilde z}}^{\min} - \omega\right)}_{\sigma}\|\tilde z_s\|^2 + \alpha_1\bar\delta\|\tilde z_s\| + 2\left(\bar a^* b + \bar d^*\right) \tag{37}$$

where $\lambda_{Q_{\tilde z}}^{\min} = \min\{a(d-c), b\}$ is the minimum eigenvalue of $Q_{\tilde z}$. We have $\sigma > 0$ when (22) holds. Thus we obtain

$$\begin{aligned}&\dot W \leq -(1-\theta)\sigma\|\tilde z_s\|^2 < 0 \\ &\forall \|\tilde z_s\| \geq \frac{\alpha_1\bar\delta + \sqrt{8\sigma\left(\bar a^* b + \bar d^*\right) - \alpha_1^2}}{2\theta\sigma}\end{aligned} \tag{38}$$

where $0 < \theta < 1$.

The main conclusion which we can draw from the considerations above is that $\tilde z_2$, which is the only state that may grow unbounded on the manifold $\mathbb{M}$, stays bounded when the external dynamics is at steady state.

Stability of the complete system

Since (25b) is GES, we have two positive definite matrices P_ξ, Q_ξ that satisfy $H_\xi^T P_\xi + P_\xi H_\xi = -Q_\xi$. Thus, we choose the following LFC

$$V = W + \kappa\,\tilde\xi^T P_\xi \tilde\xi \tag{39}$$

where W is as in (33), and $\kappa > 0$ still to be determined. Deriving (39) along the solutions of (25) we obtain

$$\dot V \leq -\tilde z_s^T Q_{\tilde z}\tilde z_s - \kappa\,\tilde\xi^T Q_\xi\tilde\xi + \frac{\partial W}{\partial \tilde z}G(\cdot)\tilde\xi + \frac{\partial W}{\partial \tilde z_2}\delta(\cdot) \tag{40}$$

The following bounds hold for $G(\cdot)$ and W:

$$G(\tilde z, \tilde\xi_3, \tilde\xi_4) \leq \bar G_1\|\tilde z_s\| + \bar G_2 \tag{41}$$

$$\left\|\frac{\partial W}{\partial \tilde z}\right\| \leq \|\tilde z_s\| \left\|\left[\begin{smallmatrix} a^2 + c + \frac{ab+d}{2} & a \\ a & 1\end{smallmatrix}\right]\right\| \leq \alpha_2\|\tilde z_s\|, \tag{42}$$

where $\bar G_1 = G_1(\bar\xi)$, $\bar G_2 = G_2(\bar\xi)$, and $\bar\xi$ is the upperbound of $\|\xi\|$. Let $\lambda_{P_{z_s}}^{\min}$, $\lambda_{P_\xi}^{\min}$, $\lambda_{Q_{\tilde z}}^{\min}$, $\lambda_{Q_\xi}^{\min}$ denote the minimal eigenvalue of P_{z_s}, P_ξ, $Q_{\tilde z}$, Q_ξ respectively. The closed-loop external dynamics (25b) is GES, therefore there exists a time t^* such that for all $t \geq t^*$: $\|\tilde\xi(t)\| \leq \lambda_{Q_{\tilde z}}^{\min}/(2\alpha_1\bar G_1)$. For $t \leq t^*$ and

$$\kappa > \frac{\alpha_1^2\bar G_2^2}{\lambda_{Q_{\tilde z}}^{\min}\lambda_{Q_\xi}^{\min}} + \frac{\alpha_1\bar G_1\bar\xi\lambda_{P_\xi}^{\min}}{\lambda_{P_{z_s}}^{\min}} \tag{43}$$

we have

$$\begin{aligned}\dot V \leq& -\tilde z_s^T Q_{\tilde z}\tilde z_s - \kappa\,\tilde\xi^T Q_\xi\tilde\xi \\ &+ \alpha_1\|\tilde z_s\|(\bar G_1\|\tilde z_s\| + \bar G_2)\tilde\xi + \alpha_1\bar\delta\|\tilde z_s\| \\ \leq& -\frac{1}{2}\lambda_{Q_{\tilde z}}^{\min}\|\tilde z_s\|^2 - \left(\frac{\alpha_1^2\bar G_2^2}{\lambda_{Q_{\tilde z}}^{\min}\lambda_{Q_\xi}^{\min}} + \frac{\alpha_1\bar G_1\bar\xi\lambda_{P_\xi}^{\min}}{\lambda_{P_{z_s}}^{\min}}\right)\lambda_{Q_\xi}^{\min}\|\tilde\xi\|^2 \\ &+ \alpha_1\bar G_1\bar\xi\|\tilde z_s\|^2 + \alpha_1\bar G_2\|\tilde z_s\|\|\tilde\xi\| \\ &- \frac{1}{2}\lambda_{Q_{\tilde z}}^{\min}\|\tilde z_s\|^2 + \alpha_1\bar\delta\|\tilde z_s\|\end{aligned} \tag{44}$$

for $\|\tilde z_s\| \geq \frac{2\alpha_1}{\lambda_{Q_z}^{\min}}$ we have

$$\begin{aligned}\dot V \leq& -\frac{1}{2}\lambda_{Q_{\tilde z}}^{\min}\|\tilde z_s\|^2 + \alpha_1\bar G_2\|\tilde z_s\|\|\tilde\xi\| \\ &- \frac{\alpha_1^2\bar G_2^2}{\lambda_{Q_{\tilde z}}^{\min}}\|\tilde\xi\|^2 - \frac{\alpha_1\bar G_1\bar\xi\lambda_{P_\xi}^{\min}}{\lambda_{P_{z_s}}^{\min}}\lambda_{Q_\xi}^{\min}\|\tilde\xi\|^2 + \alpha_1\bar G_1\bar\xi\|\tilde z_s\|^2 \\ \leq& \alpha_1\bar G_1\bar\xi\|\tilde z_s\|^2 + \frac{2\alpha_1\bar G_1\bar\xi\kappa\lambda_{P_\xi}^{\min}}{\lambda_{P_{z_s}}^{\min}}\|\tilde\xi\|^2\| \\ &\pm (ad+c)(1-\cos(\tilde z_1)) \\ \leq& \frac{2\alpha_1\bar G_1\bar\xi}{\lambda_{P_{z_s}}^{\min}}V + 2(ad+c),\end{aligned} \tag{45}$$

so for $t < t^* \wedge \|\tilde z_s\| \geq \frac{2\alpha_1}{\lambda_{Q_z}^{\min}}$ the trajectories are bounded. For $t < t^* \wedge \|\tilde z_s\| < \frac{2\alpha_1}{\lambda_{Q_z}^{\min}}$ we have $V(t)$ is bounded since ξ is bounded and $\|\tilde z_s\|$ is bounded by assumption.

For $t \geq t^*$ we have

$$\begin{aligned}\dot V \leq& -\tilde z_s^T Q_{\tilde z}\tilde z_s - \kappa\,\tilde\xi^T Q_\xi\tilde\xi + \alpha_1\|\tilde z_s\|(\bar G_1\|\tilde z_s\| + \bar G_2)\tilde\xi \\ \leq& -\frac{1}{2}\lambda_{Q_{\tilde z}}^{\min}\|\tilde z_s\|^2 + \alpha_1\bar G_2\|\tilde z_s\|\|\tilde\xi\| - \kappa\lambda_{Q_\xi}^{\min}\|\tilde\xi\|^2 \\ &- \frac{1}{2}\lambda_{Q_{\tilde z}}^{\min}\|\tilde z_s\|^2 + \alpha_1\bar\delta\|\tilde z_s\| \\ \leq& -\frac{1}{2}\lambda_{Q_{\tilde z}}^{\min}\|\tilde z_s\|^2 + \alpha_1\bar G_2\|\tilde z_s\|\|\tilde\xi\| - \kappa\lambda_{Q_\xi}^{\min}\|\tilde\xi\|^2 \\ &\forall\|\tilde z_s\| > \frac{2\alpha_1\bar\delta}{\lambda_{Q_z}^{\min}},\end{aligned} \tag{46}$$

which is negative definite for $\kappa > \alpha_1^2\bar G_2^2/(\lambda_{Q_{\tilde z}}^{\min}\lambda_{Q_\xi}^{\min})$. We can conclude that $\tilde\xi \to 0$ globally exponentially while the states z_1, z_2 are ultimately bounded. □

Now we draw our attention to straight line paths and a constant desired forward velocity. Without loss of generality, consider a path which is aligned along the x axis of the NED frame. This implies $\xi_{2_d} = \xi_{4_d} = \dot{\xi}_{4_d} = 0$. Furthermore, since we assume that the desired forward velocity is constant, we have $\dot{\xi}_{3_d} = 0$. As a result, we have $\delta(\dot{\phi}_1, \ddot{\phi}_1, \sin(\tilde{z}_1)) = 0$ and ϕ_1 is a constant angle. Under these conditions, we can derive the following corollary from Theorem 1.

Corollary 1. *Consider an under-actuated marine vehicle described by the model* (4)*, and consider the special case of control objectives* (16) *where the desired forward velocity is constant, and the desired path is a straight line. Consider the hand position point* $\mathbf{h} = [x_1, y_1]^T = [x + l\cos(\psi), y + l\sin(\psi)]^T$*, where* $[x, y]^T$ *is the position of the pivot point of the ship,* l *is a positive constant and* ψ *is the yaw angle of the vehicle. Then define* $U_d = \sqrt{(u_d - V_x)^2 + V_y^2} > 0$ *as the desired relative velocity magnitude and* $\phi = \arctan\left(\frac{-V_y}{u_d - V_x}\right)$ *as the crab angle. If Assumptions 1-8 are satisfied and if*

$$0 < \bar{U}_d < \frac{Y_2}{Y_1} \tag{47}$$

$$k_{v_i} > 0,\ k_{p_i} > 0,\ k_{I_i} > 0,\ i \in \{x, y\} \tag{48}$$

$$k_{v_i} k_{p_i} > k_{I_i} \quad i \in \{x, y\} \tag{49}$$

$$l > \max\left\{\frac{m_{22}}{m_{23}}, -\frac{X_2}{Y_2}\right\} \tag{50}$$

then the controller (12)*, where the new inputs* μ_1, μ_2 *are given by* (17)*, guarantees the achievement of the control objectives* (16)*. In particular,* $(z_1, z_2, \xi_1, \xi_2, \xi_3, \xi_4) \rightarrow (\phi, 0, u_d t, 0, u_d - V_x, -V_y)$ almost-*globally asymptotically. Furthermore, the steady state values of the integral variables give an estimate of the ocean current given by* (23).

Proof. The proof follows along the same lines as the proof of Theorem 1:

The external dynamics

The same considerations given in in the first step of Theorem 1 hold here.

The tracking dynamics

The tracking dynamics now becomes

$$\dot{\tilde{z}}_1 = \tilde{z}_2 \tag{51a}$$

$$\dot{\tilde{z}}_2 = -(a\cos(\tilde{z}_1) + b)\tilde{z}_2 - (c\cos(\tilde{z}_1) + d)\sin(\tilde{z}_1). \tag{51b}$$

The system (51) can be studied on the manifold $\mathbb{M} = \mathbb{S} \times \mathbb{R} = \{(\cos(\theta), \sin(\theta), r) \mid \theta \in \mathbb{R}, r \in \mathbb{R}\}$. The system (51) has two equilibria, and they are

$$E_s = (1, 0, 0) \in \mathbb{M}, \quad E_u = (-1, 0, 0) \in \mathbb{M}. \tag{52}$$

The point E_s is a stable node, while E_u is a saddle point since we assumed $d > c$. Note that E_u is a hyperbolic equilibrium. Choosing (33) as LFC we obtain

$$\dot{W} = -\tilde{z}_s^T Q_{\tilde{z}} \tilde{z}_s \leq 0 \qquad \forall(\sin(\tilde{z}_1), \tilde{z}_2) \neq (0, 0). \tag{53}$$

Equation (53) implies that the state $(\sin(\tilde{z}_1), \tilde{z}_2) = (0, 0)$ is GAS. However, $\sin(\tilde{z}_1) = 0$ corresponds either to $\cos(\tilde{z}_1) = 1$ or $\cos(\tilde{z}_1) = -1$ on the one-dimensional unit sphere. That is, if the vehicle is required to move along a straight line path it may move forward ($\cos(\psi) = 1$) or backwards ($\cos(\psi) = -1$). But, linearizing (51) about the origin, we have that the equilibrium $E_u = \{\cos(\tilde{z}_1), \sin(\tilde{z}_1), \tilde{z}_2) = (-1, 0, 0)\} \in \mathbb{M}$ is unstable and hyperbolic. Then, recalling [48, Theorem 3.2.1] we deduce that E_u is characterized by a stable and an unstable manifold $\mathcal{W}_u^s, \mathcal{W}_u^u$, respectively. The unstable manifold $\mathcal{W}_u^u$ is tangent to the eigenspace spanned by the positive real part eigenvalue of the Jacobian matrix of the system (51) evaluated at E_u. This manifold is therefore one-dimensional and converges to the only other equilibrium point of the system, that is $E_s = \{\cos(\tilde{z}_1), \sin(\tilde{z}_1), \tilde{z}_2) = (1, 0, 0)\} \in \mathbb{M}$. The stable manifold $\mathcal{W}_u^s$ is also one-dimensional since it is spanned by the negative real part eigenvalue of the Jacobian matrix of (51). Since the system (51) evolves on the manifold $\mathbb{M} = \mathbb{S} \times \mathbb{R}$, which is 2-dimensional (it is a "pipe-shaped" manifold, that is, it is a cylindrical surface in the space), we have that $\mathcal{W}_u^s$ has one dimension less than $\mathbb{M}$ and has therefore zero Lebesgue measure. At this point we can conclude that all the trajectories which do not start on $\mathcal{W}_u^s$ converge to the point E_s. Furthermore, since $\mathcal{W}_u^s$ has zero Lebesgue measure, we can say that E_s is *almost*-GAS.

Stability of the total system

The stability of the total system follows from Theorem 1. Choosing (39) as LFC and

$$\kappa > \alpha_1^2 \bar{G}_2^2 \left(\lambda_{Q_{\tilde{z}}}^{\min} \lambda_{Q_\xi}^{\min} + \frac{2\lambda_{Q_{\tilde{z}}}^{\min} \alpha_1 \bar{G}_1 \bar{\xi} \lambda_{P_\xi}^{\min}}{\lambda_{P_{z_s}}^{\min}}\right)^{-1} \tag{54}$$

we obtain that (46) holds $\forall \|\tilde{z}_s\|^2 > 0$. This proves that the system always converges to the equilibrium $\left(\sin(\tilde{z}_1), \tilde{z}_2, \tilde{\xi}\right) = (0, 0, \mathbf{0}_{1\times 6})$. The state $\tilde{z}_1$ converges either to $\tilde{z}_1 = 0$, or $\tilde{z}_1 = \pm\pi$, so we can conclude that $(\tilde{z}, \tilde{\xi}) = (\mathbf{0}_{1\times 2}, \mathbf{0}_{1\times 6})$ is *almost*-GAS. □

VII. Path following control

In this section a path following strategy is presented based on the hand position approach.

The path following task requires the vehicle to follow an assigned curve $\gamma(s) = \{(x(s), y(s) | s \in \mathbb{R}\}$, where s is a scalar parameter, and travel along the curve with a constant speed $U > 0$ in the global frame. This task can be fulfilled by an under-actuated vehicle if its total velocity in the NED frame $U_t = \sqrt{u^2 + v^2} = \sqrt{(\xi_3 + V_x)^2 + (\xi_4 + V_y)^2}$ is tangential to the path. The main difference between the path following task and the trajectory tracking discussed in Section IV is that for the path following the path is parametrized by a generic variable s and not necessarily by the time t. This implies that the vehicle is not required to be in a given position along the curve at a specific time instant t, but the vehicle is required just to converge to the path and move along it with a prescribed velocity.

We assume that $\gamma(s)$ is parametrized by the arc length s. Thus, the tangent vector T is a unit vector, that is

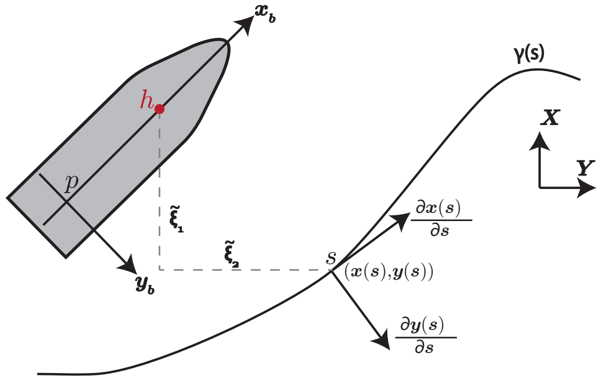

Fig. 3: Path following.

$$T = \begin{bmatrix} \frac{\partial x(s)}{\partial s} \\ \frac{\partial y(s)}{\partial s} \end{bmatrix} \wedge \|T\| = \sqrt{\left(\frac{\partial x(s)}{\partial s}\right)^2 + \left(\frac{\partial y(s)}{\partial s}\right)^2} = 1. \quad (55)$$

According to this choice of the parametrization, we can consider that a virtual frame VF, the Frenet-Serret frame [49], moves along $\gamma(s)$. The position along the curve of the origin of VF, which we call $x(s), y(s)$ is defined by the parameter s. The x axis of VF is given by the unit tangent vector to the curve, T. The y axis is given by the normal vector N and it is chosen by rotation of T by $\pi/2$ radians. The velocity in the NED frame with which VF moves along $\gamma(s)$ is given by

$$\mathbf{U}_{VF} = [\dot{x}(s), \dot{y}(s)] = \left[\frac{\partial x(s)}{\partial s}\dot{s}, \frac{\partial y(s)}{\partial s}\dot{s}\right]. \quad (56)$$

Note that the total velocity of VF in the NED frame is

$$U_{VF} = \dot{s}\sqrt{\left(\frac{\partial x(s)}{\partial s}\right)^2 + \left(\frac{\partial y(s)}{\partial s}\right)^2} = \dot{s} \quad (57)$$

because of our choice of the parametrization for $\gamma(s)$. Notice that $\dot{s}$ is left as design parameter to be chosen in the following.

We consider the following assumption to hold

Assumption 9. *The path $\gamma(s)$ is a $\mathcal{C}^2$ function.*

Remark 9. *This assumption implies that*

$$\frac{\partial x(s)}{\partial s}, \frac{\partial y(s)}{\partial s}, \frac{\partial^2 x(s)}{\partial s^2}, \frac{\partial^2 x(s)}{\partial s^2}$$

are all continuous. Therefore, the curvature κ of $\gamma(s)$ is continuous and the curve is smooth.

The control objectives can be formalized as follows

$$\lim_{t\to\infty}(\xi_1 - x(s)) = 0 \quad (58a)$$
$$\lim_{t\to\infty}(\xi_2 - y(s)) = 0 \quad (58b)$$
$$\lim_{t\to\infty}(U_t - U) = 0 \quad (58c)$$

The control objectives (58) mean that we want the total velocity of the vehicle U_t converge to a constant value U, while the point $\mathbf{h}$ has to converge to the origin of VF, i.e., $(\xi_1, \xi_2) \to (x(s), y(s))$ (see Figure 3).

In order to fulfill the control objectives (58) we introduce the following controller for (13)

$$\begin{aligned} \mu_1 = &- k_{v_x}(\xi_3 - \dot{x}(s)) - k_{p_y}(\xi_1 - x(s)) \\ &- k_{I_x}\left(\xi_{1_I} - \int_0^t x(s)\mathrm{d}\tau\right) + \ddot{x}^*(s) \end{aligned} \quad (59a)$$

$$\begin{aligned} \mu_2 = &- k_{v_y}(\xi_4 - \dot{y}(s)) - k_{p_y}(\xi_2 - y(s)) \\ &- k_{I_y}\left(\xi_{2_I} - \int_0^t x(s)\mathrm{d}\tau\right) + \ddot{y}^*(s) \end{aligned} \quad (59b)$$

where

$$\dot{x}(s) = \dot{s}\,\frac{\partial x(s)}{\partial s} \qquad \ddot{x}^*(s) = \dot{s}\,U\,\frac{\partial^2 x(s)}{\partial^2 s} \quad (60)$$

$$\dot{y}(s) = \dot{s}\,\frac{\partial y(s)}{\partial s} \qquad \ddot{y}^*(s) = \dot{s}\,U\,\frac{\partial^2 y(s)}{\partial^2 s}. \quad (61)$$

The terms $\ddot{x}^*(s)$, $\ddot{y}^*(s)$ are two feed-forward terms and $\ddot{x}^*(s) \neq \ddot{x}(s)$, $\ddot{y}^*(s) \neq \ddot{x}(s)$. We cannot choose $\ddot{x}(s), \ddot{y}(s)$ as feed-forward terms since their expressions depend on $\ddot{s}$, which in turn depends on V_x, V_y, that are unknown. We have the freedom to choose the dynamics of s such that the path following task is fulfilled. We choose

$$\dot{s} = U\left(1 - \epsilon\tanh(\sqrt{\tilde{\xi}_1^2 + \tilde{\xi}_2^2}\right) \quad (62)$$

where $U > 0$ is the desired total velocity of the vehicle when traveling along the curve, $\epsilon > 0$ is a constant and $\tilde{\xi}_1 = \xi_1 - x(s), \tilde{\xi}_2 = \xi_2 - y(s)$. The chosen parametrization (62) means that the frame VF slows down when the vehicle is far from $\gamma(s)$ and has constant forward velocity U when the vehicle is on $\gamma(s)$. This approach facilitates the vehicle to catch up with VF when the euclidean distance between the vehicle and VF, i.e., $\sqrt{\tilde{\xi}_1^2 + \tilde{\xi}_2^2}$, is large.

The following theorem presents the main result for the path following strategy.

Theorem 2. *Consider an under-actuated marine vehicle described by the model* (4). *Consider the hand position point $\mathbf{h} = [x_1, y_1]^T = [x + l\cos(\psi), y + l\sin(\psi)]^T$, where $[x, y]^T$ is the position of the pivot point of the ship, l is a positive constant and ψ is the yaw angle of the vehicle. Then define $U_{d_\gamma} = \sqrt{\left(U\frac{\partial x_\gamma(s)}{\partial s} - V_x\right)^2 + \left(U\frac{\partial y_\gamma(s)}{\partial s} - V_y\right)^2} > 0$ as the desired relative velocity magnitude and $\phi_{1_\gamma} = \arctan\left(\frac{U\frac{\partial x_\gamma(s)}{\partial s} - V_y}{U\frac{\partial y_\gamma(s)}{\partial s} - V_x}\right)$ as the crab angle. If Assumptions 1-6 and 9, inequalities (18-21) are satisfied and if*

$$U_{d_\gamma} > 0 \qquad \epsilon < \frac{\lambda_Q^{\min}}{2\lambda_P^{\max}} \quad (63a)$$

$$\kappa \leq \frac{2\min\{\underline{a}(\underline{d} - \underline{c}), b\}}{\left(\frac{Y_1 \bar{U}_d}{l} + 2\left(Y_1 - \frac{X_1 - 1}{l}\right)\right)U} \quad (63b)$$

then the controller (12), *where the new inputs μ_1, μ_2 are given by* (59), *guarantees the achievement of the control objectives* (58).

Remark 10. *Note that for the path following case, the stability of the system depends on a bound on the curvature κ rather than on a bound on the desired acceleration $\dot{U}_d$. This difference is clear from the definition of U_{d_γ}. In fact, according to the parametrization defined above, the time derivative of U_{d_γ} is $\dot{U}_{d_\gamma} = \kappa \dot{s}$. In fact, since we define a desired constant tangential velocity U, the desired velocity U_{d_γ} changes only according to the change of the curvature of $\gamma(s)$.*

Proof. We prove that choosing the dynamics $\dot{s}$ as in (62), the external dynamics globally exponentially fulfills the objectives (58). The stability of the tracking dynamics follows along the same lines as the proof of Theorem 1.

The external dynamics

First we define the following change of coordinates

$$\tilde{\xi}_{1_I} = \xi_{1_I} - \int_0^t x(s)\mathrm{d}\tau - \frac{k_{I_x} V_x}{k_{v_x}} \tag{64}$$

$$\tilde{\xi}_{2_I} = \xi_{2_I} - \int_0^t y(s)\mathrm{d}\tau - \frac{k_{I_y} V_y}{k_{v_y}} \tag{65}$$

$$\tilde{\xi}_1 = \xi_1 - x(s) \quad \tilde{\xi}_3 = \xi_3 - \left(U \frac{\partial x(s)}{\partial s} - V_x\right) \tag{66}$$

$$\tilde{\xi}_2 = \xi_2 - y(s) \quad \tilde{\xi}_4 = \xi_4 - \left(U \frac{\partial y(s)}{\partial s} - V_y\right). \tag{67}$$

We obtain

$$\dot{\tilde{\xi}} = H_{\tilde{\xi}} \tilde{\xi} + \Delta_{pf}(\tilde{\xi}_1, \tilde{\xi}_2) \tag{68}$$

with $\tilde{\xi} = [\tilde{\xi}_{1_I}, \tilde{\xi}_{2_I}, \tilde{\xi}_1, \tilde{\xi}_2, \tilde{\xi}_3, \tilde{\xi}_4]^T$, $H_{\tilde{\xi}}$ like in (31) and

$$\Delta_{pf}(\cdot) = \epsilon \begin{bmatrix} 0 \\ 0 \\ \frac{\partial x(s)}{\partial s} \tanh\left(\sqrt{\tilde{\xi}_1^2 + \tilde{\xi}_2^2}\right) \\ \frac{\partial y(s)}{\partial s} \tanh\left(\sqrt{\tilde{\xi}_1^2 + \tilde{\xi}_2^2}\right) \end{bmatrix}. \tag{69}$$

Note $\Delta_{pf}(0,0) = \mathbf{0}$ and

$$\|\Delta_{pf}(\cdot)\| \le \epsilon \left\| \left[\frac{\partial x(s)}{\partial s}, \frac{\partial y(s)}{\partial s} \right] \right\| \|\tilde{\xi}\| \le \epsilon \|\tilde{\xi}\|. \tag{70}$$

Since $H_{\tilde{\xi}}$ is Hurwitz because of (19-20) we have that there exists a positive definite matrix P which satisfies $H_{\tilde{\xi}}^T P + P^T H_{\tilde{\xi}} = -Q$ for Q being a positive definite matrix. Choosing the following LFC

$$V_{pf} = \tilde{\xi}^T P \tilde{\xi} \tag{71}$$

we have

$$\dot{V}_{pf} = -\tilde{\xi}^T Q \tilde{\xi} + \frac{\partial V_{pf}}{\partial \tilde{\xi}} \Delta_{pf}(\cdot) \tag{72}$$

$$\le -\lambda_Q^{\min} \|\tilde{\xi}\|^2 + 2\epsilon \lambda_P^{\max} \|\tilde{\xi}\|^2 \tag{73}$$

which is negative definite choosing $\epsilon < \frac{\lambda_Q^{\min}}{2\lambda_P^{\max}}$. Then we have that $\|\tilde{\xi}\| = 0$ is GES.

The internal dynamics

For the internal dynamics we define $\tilde{z}_1 = z_1 - \phi_{1_\gamma}$ and $\tilde{z}_2 = z_2 - \dot{\phi}_{1_\gamma}$. Then we obtain the same form as in (25a) where the definition of a, b, c, d is the same as in (29) but with U_{d_γ} in place of U_d. The proof that z_1, z_2 are bounded follows along the lines of the proof of Theorem 1 defining a LFC as in (33). Note that the time derivative of a, b, c and d are also in this case nonzero since $\dot{U}_{d_\gamma} \neq 0$. However, according to (63b), we have $\dot{U}_{d_\gamma} \le \bar{U}^*_{d_\gamma}$, where $\bar{U}^*_{d_\gamma}$ is a positive constant. Then the proof follows from the one given in Section VI.

Stability of the complete system

The stability of the complete system follows along the same lines as the proof of Theorem 1. ☐

Remark 11. *The path following strategy presented here is a generalization of the one presented in [43]. In particular, the approach presented here and based on the parametrization* (62) *can be specialized to the case of straight line paths in [43]. Without loss of generality we can consider here the case of straight line path aligned with x axis of the NED frame. Then a straight line path can be represented as $\gamma_{strt} = \{(s, 0) : s \in \mathbb{R}\}$. Generally, straight line paths are left unparametrized for path following tasks, e.g. [30, 50]. This corresponds to the case of $\epsilon = 0$ and $k_{p_x} = k_{I_x} = 0$ in the controller* (59), *i.e., leaving the state ξ_1 uncontrolled, regulating ξ_2 to 0 and controlling ξ_3, ξ_4 such that $\sqrt{u^2 + v^2} \to U$. It is then possible to verify that the state $z_2 \to 0$ and $z_1 \to \arctan\left(\frac{V_y}{U - V_x}\right)$ [43]. The angle $\phi = \arctan\left(\frac{V_y}{U - V_x}\right)$ is called the crab angle, and it is necessary when a disturbance affects under-actuated vehicles in order to compensate for it [38]. Finally, note that in the case of unparametrized path following it is not possible to estimate the ocean current as in* (23) *since we do not have a position reference in the along-path direction.*

VIII. Simulation Results

In this section we present a simulation case study concerning the trajectory tracking control problem in order to validate the theoretical results presented above. For the simulation we use the mathematical model of the LAUV (light autonomous underwater vehicle, see Figure 10) given in [44] and developed by Laboratorio de Sistemas e Tecnologia Subaquatica (LSTS) at University of Porto. This simulation was performed using MATLAB. The vehicle is required to move along a lawn-mower path made of three straight lines of length $l_1 = 150$ [m] connected by two circular arcs with radius $R = 30$ [m]. The temporal constraint requires the vehicle to be at the time instant $t = 0$ [s] at the position $(x, y) = (0, 0)$ and at the time instant $t = 638$ [s] at the position $(x, y) = (150, 60)$ while keeping a constant forward velocity $U_d = 1$ [m/s] during the motion. In the simulation we assign an ocean current $\mathbf{V} = [V_x, V_y]^T = [0.05, -0.08]^T$ [m/s] which is unknown to the vehicle. For the point $\mathbf{h}$ we choose $l = 1$ [m]. The gains for the controller (17) are $k_{v_x} = k_{v_y} = 50$, $k_{p_x} = k_{p_y} = 5$, $k_{I_x} = k_{I_y} = 0.5$. Finally, we consider that the forward thrust $T_u \in [-T_u^{\max}(u_r), T_u^{\max}(u_r)]$ is dynamically saturated with

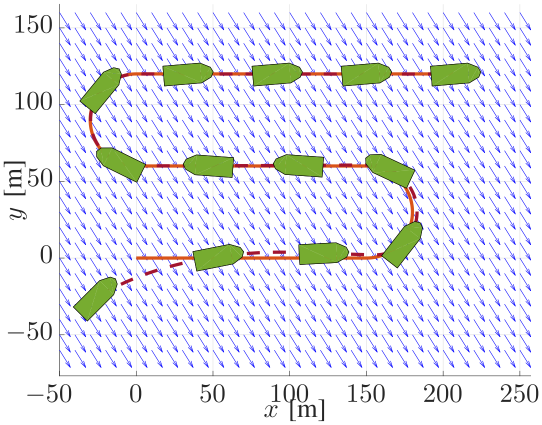

Fig. 4: Motion of the vehicle.

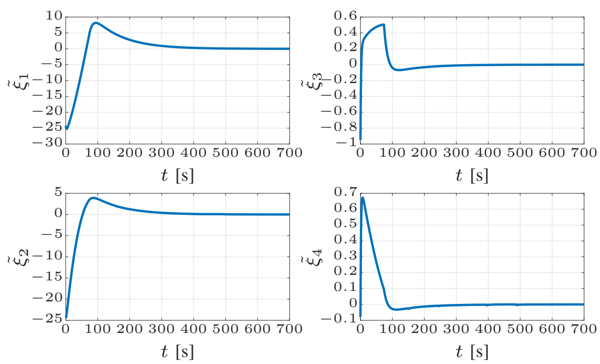

Fig. 5: Error states and ocean current estimates.

saturation limits given by $T_u^{\max} = T_{nn}n_{\max}^2 - T_{un}n_{\max}u_r$, where $n_{\max} = 2500/60$ [rps], $T_{nn} = 0.0096$, and $T_{un} = 0.126$ and the rudder angle T_r is limited to 25° [44]. Figure 4 shows the motion of the vehicle and we see that the vehicle converges to the trajectory. In Figure 5, we see that the error states (24) converge to zero. Figure 6 shows the ocean current estimates according to (23), and we see that they converge to the actual values. Finally, Figure 7 shows the surge thrust T_u, and the rudder angle T_r where we notice that they are both saturated during the initial phase of the motion.

IX. Sea trial results

This section is divided into two subsections in which we first present a simulation performed with the simulator of

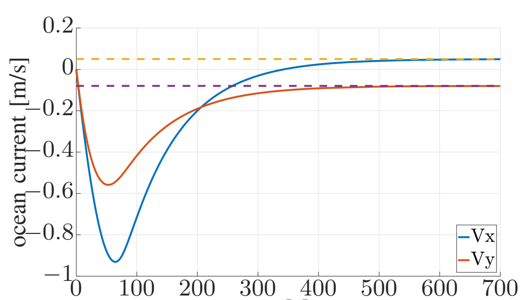

Fig. 6: Ocean current estimates.

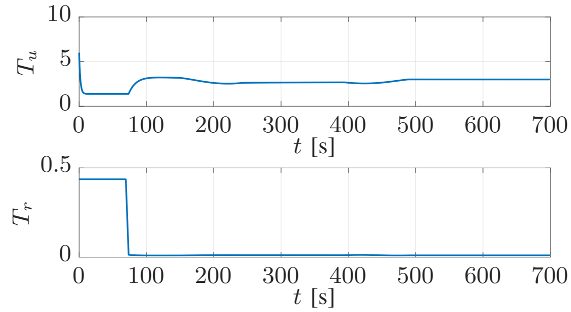

Fig. 7: Surge thrust T_u, and rudder angle T_r.

DUNE [45]. DUNE is the software running on the LAUVs and is developed by the LSTS. The control algorithm presented above has been implemented in DUNE in order to perform experiments and validate the theoretical results presented in this paper concerning the path following control problem. Furthermore, before performing the sea trials, simulations were performed using the simulator of DUNE in order to verify that the control algorithm was behaving correctly once implemented in the real system. DUNE has a very detailed model of the LAUV and there are nodes in the software which realistically simulate the behavior of the sensors on-board the real vehicle, i.e., they also simulate measurement noise. The result of this simulation is used as a benchmark for the sea trial presented in the second subsection of Section IX. The experiments were conducted in the harbor of Porto, Portugal. We remark that the sea trials have concerned the particular case of the straight line path following control problem since this is what we could implement in DUNE

DUNE simulation

As regards the desired motion, the vehicle is required to move with a constant forward velocity of $U_d = 1.2$ [m/s] while traveling along a lawn-mower path made of four long straight lines $l_1 = 130$ [m] connected by three perpendicular straight lines $l_2 = 27$ [m]. The simulation is performed underwater and the depth of the path is set to 2 [m] under the surface. We do not implement any depth controller but rather use the depth controller already available in DUNE. Note that the path respects the assumptions of Theorem 2 along the straight line segments. The choice of such a kind of path is driven by the fact that lawn-mower paths are standard for marine vehicles when required to execute surveillance and scanning tasks in the ocean. Since we have chosen a lawn-mower path we decide to deal with the case of unparametrized paths as discussed in Remark 11, i.e., we define $k_{p_x} = k_{I_x} = \epsilon = 0$. The other gains are $k_{v_x} = k_{v_y} = 1, k_{p_y} = 0.2, k_{I_y} = 0.01$.

In the simulation we assign an ocean current $\mathbf{V} = [V_x, V_y]^T = [0.1, 0.2]^T$ [m/s] which is unknown to the vehicle. We remark that in the case of path following it is not possible to estimate the ocean current according to (23) since we do not have any reference velocity along the global x-axis. For the point $\mathbf{h}$ we choose $l = 1$ [m].

Figure 8 shows the motion of the vehicle, and it is readily seen from this figure that the path following task is fulfilled.

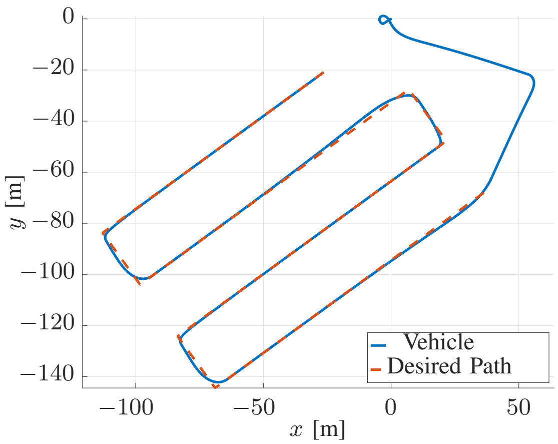

Fig. 8: Motion of the vehicle in the real trial.

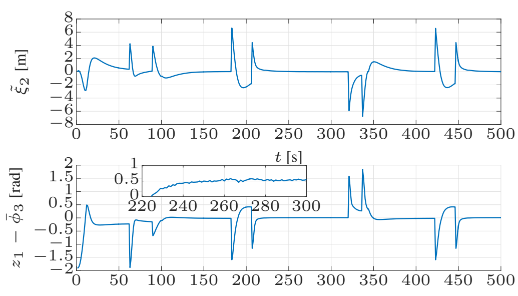

Fig. 9: Top) Cross-track error in the sea trial; Bottom) Course error in the sea trial.

Note that along the short side of the path the transient is not long enough in order to have $\tilde{\xi}_2 \to 0$. This is not a problem for real applications, e.g. sonar scanning, since the data collection is performed along the long sides of the path. In Figure 9, the cross-track error, i.e., the state $\tilde{\xi}_2$, is shown and we see that along the long side of the path it converges to zero. As mentioned in Remark 11, Figure 9 shows also the state $\tilde{z}_1 = \psi - \phi$ converging to a constant $\phi = \left(\frac{V_y^{\text{cross}}}{U}\right)$, i.e., the crab angle, where V_y^{cross} is the component of $\mathbf{V}$ acting in the perpendicular direction w.r.t. the straight line the vehicle is traveling. We have zoomed the behavior in the range $(200, 300)$[s] which characterizes the motion of the vehicle in the North-East direction. Note that $\tilde{z}_1 \to 0.5°$ and we expect $\phi = 0.6°$. We have $\tilde{z}_1 \neq \phi$ due to the presence of simulated sensor noise in DUNE.

Sea trial

The task assignment for the vehicle is the same as the one discussed in the previous subsection. We remark that the sea trial has been performed at a constant depth of 2 [m]. However, as already mentioned, we used the depth controller already available in DUNE. Note that GPS measurements are not available underwater. Thus, we used the position estimates provided by the navigation system available in DUNE which are based on Kalman filters and measurements from the on-board IMU.

Fig. 10: Light autonomous underwater vehicle (LAUV).

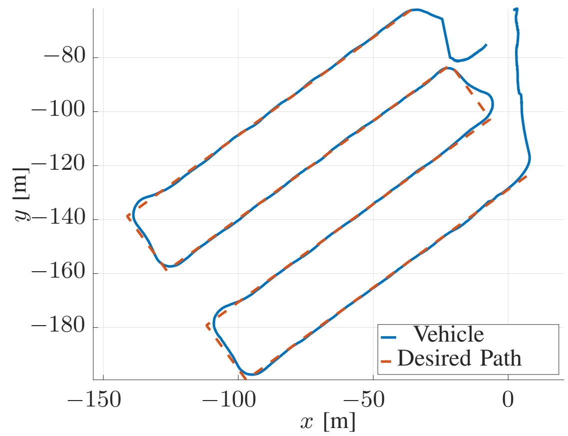

Fig. 11: Motion of the vehicle in the real trial.

In the real trial we do not know the value of the ocean current so we cannot compute the expected angle ϕ. Note also that according to Remark 11 we cannot estimate the ocean current V for the path following case.

Figure 11 shows the motion of the vehicle compared to the desired trajectory. We see that the vehicle fulfills the path following task. This is also confirmed by Figure 12 where the cross-track error is reported, and it is possible to see how it converges to zero during the motion along the long sides of the path.

From Figures 11-12, it is also clear that the behavior of the

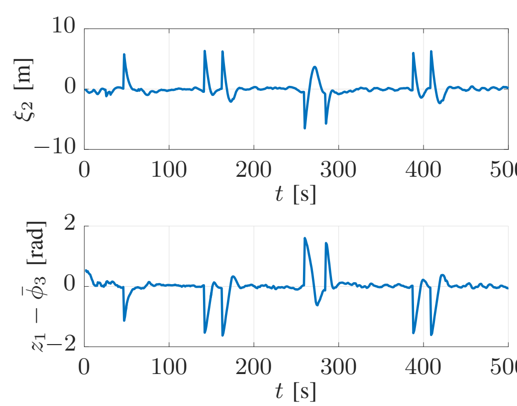

Fig. 12: Top) Cross-track error in the sea trial; Bottom) Course error in the sea trial.

vehicle from the experimental results is in line with what to expect from the simulations.

X. Conclusions

In this paper we have presented a trajectory tracking and a path following control strategy for under-actuated marine vehicles. In particular, we have considered the model of an ASV or an AUV moving in the horizontal plane. Inspired by works on ground vehicles which have introduced the definition of the *hand position* point for UGVs, we have extended this concept to marine vehicles. We applied the input-output feedback linearization method using the *hand position* as output and developed a trajectory tracking and a path following strategy for generic paths, with straight line paths as a special case. During the analysis we have considered that environmental disturbances, e.g., constant and irrotational ocean current, affect the vehicle. Rigorous mathematical proofs for the stability of the closed-loop system have been given. The theoretical results are validated by both simulations and experimental results have also been presented in order to validate the theoretical results.

Appendix A
Equations

$$F_{u_r}(v_r, r) \triangleq \frac{1}{m_{11}}(m_{22}v_r + m_{23}r)r - \frac{d_{11}}{m_{11}}u_r, \tag{74}$$

$$X_1(\mathbf{M}) \triangleq \frac{m_{11}m_{33}-m_{23}^2}{m_{22}m_{33}-m_{23}^2} \quad X_2(\mathbf{M},\mathbf{D}) \triangleq \frac{d_{33}m_{23}-d_{23}m_{33}}{m_{22}m_{33}-m_{23}^2} \tag{75}$$

$$Y_1(\mathbf{M}) \triangleq \frac{(m_{11}-m_{22})m_{23}}{m_{22}m_{33}-m_{23}^2} \quad Y_2(\mathbf{M},\mathbf{D}) \triangleq \frac{d_{22}m_{33}-d_{32}m_{23}}{m_{22}m_{33}-m_{23}^2} \tag{76}$$

$$X(u_r) \triangleq -X_1u_r + X_2 \quad Y(u_r) \triangleq -Y_1u_r - Y_2, \tag{77}$$

$$\begin{aligned} F_r(u_r, v_r, r) \triangleq& \frac{m_{23}d_{22}-m_{22}(d_{32}+(m_{22}-m_{11})u_r)}{m_{22}m_{33}-m_{23}^2}v_r \\ &+\frac{m_{23}(d_{23}+m_{11}u_r)-m_{22}(d_{33}+m_{23}u_r)}{m_{22}m_{33}-m_{23}^2}r, \end{aligned} \tag{78}$$

$$G(\tilde{z}, \tilde{\xi}_3, \tilde{\xi}_4) \triangleq \begin{bmatrix} \mathbf{0} & 0 & 0 \\ \mathbf{g}(\tilde{z}_1) & \alpha(\tilde{z},\tilde{\xi}_3) & \beta(\tilde{z},\tilde{\xi}_3,\tilde{\xi}_4) \end{bmatrix} \tag{79}$$

$$\mathbf{g}(\tilde{z}_1) = \begin{bmatrix} k_{I_x}\sin(\tilde{z}_1)l & -\frac{k_{I_y}\cos(\tilde{z}_1)}{l} & \frac{k_{P_x}\sin(\tilde{z}_1)}{l} & -\frac{k_{P_y}\cos(\tilde{z}_1)}{l} \end{bmatrix} \tag{80}$$

$$\begin{aligned} \alpha(\tilde{z}, \tilde{\xi}_3) \triangleq& -\left(\left(Y_1 - \frac{X_1-1}{l}\right)z_2 + \frac{Y_1U_d\sin(\tilde{z}_1)}{l}\right)\cos(z_1) \\ &\left(-\frac{Y_1U_d\cos(\tilde{z}_1)}{l} - \frac{Y_2}{l} - \frac{Y_1\left(\tilde{\xi}_3\cos(z_1)+\tilde{\xi}_4\sin(z_1)\right)}{l}\right. \\ &\left.+\frac{k_{v_x}}{l}\right)\sin(\tilde{z}_1+\phi_1) \end{aligned} \tag{81}$$

$$\begin{aligned} \beta(\tilde{z}, \tilde{\xi}_3, \tilde{\xi}_4) \triangleq& -\left(\left(Y_1 - \frac{X_1-1}{l}\right)z_2 + \frac{Y_1U_d\sin(\tilde{z}_1)}{l}\right)\sin(z_1) \\ &\left(-\frac{Y_1U_d\cos(\tilde{z}_1}{l} - \frac{Y_2}{l} - \frac{Y_1\left(\tilde{\xi}_3\cos(z_1)+\tilde{\xi}_4\sin(z_1)\right)}{l}\right. \\ &\left.+\frac{k_{v_y}}{l}\right)\cos(\tilde{z}_1+\phi_1) \end{aligned} \tag{82}$$

References

[1] K. Jo, J. Kim, D. Kim, C. Jang, and M. Sunwoo, "Development of autonomous car - part I: distributed system architecture and development process," *IEEE Transactions on Industrial Electronics*, vol. 61, no. 12, pp. 7131–7140, 2014.

[2] ——, "Development of autonomous car - part II: A case study on the implementation of an autonomous driving system based on distributed architecture," *IEEE Transactions on Industrial Electronics*, vol. 62, no. 8, pp. 5119–5132, 2015.

[3] D. Shim, H. Chung, H. J. Kim, and S. Sastry, "Autonomous exploration in unknown urban environments for unmanned aerial vehicles," in *Proc. AIAA Guidance, Navigation, Control Conf. Exhibit*, San Francisco, CA, 2005.

[4] I. Colomina and P. Molina, "Unmanned aerial systems for photogrammetry and remote sensing: A review," *ISPRS Journal of Photogrammetry and Remote Sensing*, vol. 92, pp. 79–97, 2014.

[5] D. Kingston, R. W. Beard, and R. S. Holt, "Decentralized perimeter surveillance using a team of UAVs," *IEEE Transactions on Robotics*, vol. 24, no. 6, pp. 1394–1404, 2008.

[6] D. Goldberg, V. Cicirello, M. B. Dias, R. Simmons, S. Smith, T. Smith, and A. Stentz, "A distributed layered architecture for mobile robot coordination: Application to space exploration," in *Proc. International NASA Workshop on Planning and Scheduling for Space*, Houston, Texas, USA, 2002.

[7] Y. Cheng, M. W. Maimone, and L. Matthies, "Visual odometry on the mars exploration rovers - a tool to ensure accurate driving and science imaging," *IEEE Robotics & Automation Magazine*, vol. 13, no. 2, pp. 54–62, 2006.

[8] R. A. Lindemann and C. J. Voorhees, "Mars exploration rover mobility assembly design, test and performance," in *Proc. IEEE International Conference on Systems, Man and Cybernetics*, Waikoloa, HI, USA, 10-12 Oct, 2005, pp. 450–455.

[9] M. Ludvigsen, G. Johnsen, P. Lågstad, A. Sørensen, and Ø. Ødegård, "Scientific operations combining ROV and AUV in the Trondheim Fjord," in *Proc. of OCEANS*, Bergen, Norway, 2013, pp. 1–7.

[10] D. Ribas, N. Palomeras, P. Ridao, M. Carreras, and A. Mallios, "Girona 500 AUV: From survey to intervention," *IEEE ASME Transactions on Mechatronics*, vol. 17, no. 1, p. 46, 2012.

[11] A. D. Bowen, D. R. Yoerger, C. Taylor, R. McCabe, J. Howland, D. Gomez-Ibanez, J. C. Kinsey, M. Heintz, G. McDonald, D. B. Peters *et al.*, "The nereus hybrid underwater robotic vehicle for global ocean science operations to 11,000 m depth," in *Proc. of OCEANS*, Quebec City, QC, Canada, 2008.

[12] M. S. Triantafyllou and F. S. Hover, "Maneuvering and control of marine vehicles," *Cambridge, Massachusetts, USA*, 2003.

[13] O. Faltinsen, *Sea loads on ships and offshore structures*. Cambridge university press, 1993, vol. 1.

[14] T. A. Johansen and T. I. Fossen, "Control allocationa survey," *Automatica*, vol. 49, no. 5, 2013.

[15] A. Alessandretti, A. P. Aguiar, and C. Jones, "Trajectory-tracking and path-following controllers for constrained

underactuated vehicles using model predictive control," in *Proc. IEEE European Control Conference,*, Zurich, Switzerland, 17-19 July, 2013, pp. 1371–1376.

[16] M. Abdelaal, M. Fränzle, and A. Hahn, "Nonlinear model predictive control for tracking of underactuated vessels under input constraints," in *Proc. IEEE European Modelling Symposium*, Madrid, Spain, 6-8 Oct., 2015.

[17] B. J. Guerreiro, C. Silvestre, R. Cunha, and A. Pascoal, "Trajectory tracking nonlinear model predictive control for autonomous surface craft," *IEEE Transactions on Control Systems Technology,*, vol. 22, no. 6, pp. 2160–2175, 2014.

[18] A. P. Aguiar, J. P. Hespanha *et al.*, "Trajectory-tracking and path-following of underactuated autonomous vehicles with parametric modeling uncertainty," *IEEE Transactions on Automatic Control*, vol. 52, no. 8, pp. 1362–1379, 2007.

[19] Z.-P. Jiang, "Global tracking control of underactuated ships by Lyapunov's direct method," *Automatica*, vol. 38, no. 2, pp. 301–309, 2002.

[20] K. Do and J. Pan, "Global tracking control of underactuated ships with nonzero off-diagonal terms in their system matrices," *Automatica*, vol. 41, no. 1, pp. 87–95, 2005.

[21] K. Pettersen and H. Nijmeijer, "Tracking control of an underactuated surface vessel," in *Proc. 37th IEEE Conference on Decision and Control*, Tampa, Florida, USA, Dec. 1998, pp. 4561–4566.

[22] K. Y. Pettersen and H. Nijmeijer, "Semi-global practical stabilization and disturbance adaptation for an underactuated ship," in *Proc. of the 39th IEEE Conference on Decision and Control*, vol. 3, 2000, pp. 2144–2149.

[23] E. Lefeber, K. Y. Pettersen, and H. Nijmeijer, "Tracking control of an underactuated ship," *IEEE Transactions on Control Systems Technology*, vol. 11, no. 1, pp. 52–61, 2003.

[24] D. J. W. Belleter, M. Maghenem, C. Paliotta, and K. Y. Pettersen, "Observer based path following for underactuated marine vessels in the presence of ocean currents: a global approach," *Submitted to Automatica - https://www.dropbox.com/s/f6u9gysdp9wuiiq/ Journal-Glo.pdf?dl=0*, 2017.

[25] C. P. Bechlioulis, G. C. Karras, S. Heshmati-Alamdari, and K. J. Kyriakopoulos, "Trajectory tracking with prescribed performance for underactuated underwater vehicles under model uncertainties and external disturbances," *IEEE Transactions on Control Systems Technology*, vol. 25, 2017.

[26] T. I. Fossen, M. Breivik, and R. Skjetne, "Line-of-sight path following of underactuated marine craft," in *Proc. 6th IFAC Inter. Conf. on Maneuvering and Control of Marine Crafts*, Girona, Spain, 2003.

[27] E. Fredriksen and K. Y. Pettersen, "Global κ-exponential way-point manoeuvering of ships," in *Proc. 43rd IEEE Conference on Decision and Control*, Atlantis, Bahamas, Dec. 14-17, 2004.

[28] E. Børhaug, A. Pavlov, and K. Y. Pettersen, "Integral LOS control for path following of underactuated marine surface vessels in the presence of constant ocean currents," in *Proc. 47th IEEE Conference on Decision and Control*, Cancun, Mexico, Dec. 9-11, 2008, pp. 4984–4991.

[29] E. Børhaug, A. Pavlov, E. Panteley, and K. Y. Pettersen, "Straight line path following for formations of underactuated marine surface vessels," *IEEE Transaction on Control Systems Technology*, vol. 19, no. 3, 2011.

[30] W. Caharija, K. Y. Pettersen, M. Bibuli, P. Calado, E. Zereik, J. Braga, J. T. Gravdahl, A. J. Sørensen, M. Milovanović, and G. Bruzzone, "Integral line-of-sight guidance and control of underactuated marine vehicles: Theory, simulations, and experiments," *IEEE Transactions on Control Systems Technology*, vol. 24, no. 5, pp. 1623–1642, 2016.

[31] P. Maurya, A. P. Aguiar, and A. Pascoal, "Marine vehicle path following using inner-outer loop control," in *Proc. 8th IFAC Inter. Conf. on Manoeuvring and Control of Marine Craft*, Guaruj, Brazil, 2009, pp. 38–43.

[32] M. Burger, A. Pavlov, and K. Pettersen, "Conditional integrators for path following and formation control of marine vessels under constant disturbances," in *Proc. 8th IFAC Inter. Conf. on Manoeuvring and Control of Marine Craft, Guaruj, Brazil*, 2009, pp. 179–184.

[33] D. Belleter, C. Paliotta, M. Maggiore, and K. Pettersen, "Path following for underactuated marine vessels," in *Proc. 10th IFAC Symposium on Nonlinear Control Systems*, Monterey, CA, USA 2016.

[34] L. Lapierre and D. Soetanto, "Nonlinear path-following control of an auv," *Ocean Engineering*, vol. 34, no. 11, pp. 1734–1744, 2007.

[35] T. I. Fossen and K. Y. Pettersen, "On uniform semiglobal exponential stability (USGES) of proportional line-of-sight guidance laws," *Automatica*, vol. 50, no. 11, 2014.

[36] K. D. Do and J. Pan, "State-and output-feedback robust path-following controllers for underactuated ships using serret-frenet frame," *Ocean Engineering*, vol. 31, no. 5, pp. 587–613, 2004.

[37] S. Moe, W. Caharija, K. Y. Pettersen, and I. Schjølberg, "Path following of underactuated marine surface vessels in the presence of unknown ocean currents," in *Proc. IEEE American Control Conference*, 2014, pp. 3856–

3861.

[38] T. I. Fossen, *Handbook of marine craft hydrodynamics and motion control*. John Wiley & Sons, 2011.

[39] M. S. Wiig, K. Y. Pettersen, and T. R. Krogstad, "Uniform semiglobal exponential stability of integral line-of-sight guidance laws," in *10th IFAC Iner. Conf. on Conference on Maneuvering and Control of Marine Craft*, Copenaghen, Denmark, Aug. 2015, pp. 61–68.

[40] E. J. Rodríguez-Seda, C. Tang, M. W. Spong, and D. M. Stipanović, "Trajectory tracking with collision avoidance for nonholonomic vehicles with acceleration constraints and limited sensing," *The International Journal of Robotics Research*, vol. 33, no. 12, pp. 1569–1592, 2014.

[41] J. R. Lawton, R. W. Beard, and B. J. Young, "A decentralized approach to formation maneuvers," *IEEE Transactions on Robotics and Automation*, vol. 19, no. 6, pp. 933–941, 2003.

[42] C. Paliotta and K. Y. Pettersen, "Leader-follower synchronization with disturbance rejection," in *IEEE Multi-Conference on Systems and Control*, Buenos Aires, Argentina, Sep. 2016.

[43] C. Paliotta, E. Lefeber, and K. Y. Pettersen, "Trajectory tracking of under-actuated marine vehicles," in *Proc. 45th IEEE Conference on Decision and Control*, Las Vegas, Nevada, USA, Dec. 2016.

[44] J. E. da Silva, B. Terra, R. Martins, and J. B. de Sousa, "Modeling and simulation of the LAUV autonomous underwater vehicle," in *Proc. 13th IFAC Inter. Conf. on Methods and Models in Automation and Robotics*, Szczecin, Poland, Aug., 2007.

[45] L. de Sistemas e Tecnologia Subaquatica (LSTS). (2015) Dune: unified navigation environment,. [Online]. Available: http://lsts.fe.up.pt/toolchain/dune

[46] H. K. Khalil, *Nonlinear systems*, 3rd ed. Prentice hall New Jersey, 2000.

[47] K. J. Aström and R. M. Murray, *Feedback systems: An Introduction for Scientists and Engineers*. Princeton university press, 2010.

[48] J. Guckenheimer and P. J. Holmes, *Nonlinear oscillations, dynamical systems, and bifurcations of vector fields*. Springer Science & Business Media, 2013, vol. 42.

[49] O. Egeland and J. T. Gravdahl, *Modeling and simulation for automatic control*. Marine Cybernetics Trondheim, Norway, 2002, vol. 76.

[50] W. Caharija, K. Y. Pettersen, J. T. Gravdahl, and E. Borhaug, "Integral LOS guidance for horizontal path following of underactuated autonomous underwater vehicles in the presence of vertical ocean currents," in *Proc. 2012 American Control Conference*, Montreal, Canada, June 2012, pp. 5427–5434.